LACE
nwp central europe

# Report from stay in Prague January 2025
# Overview of new dynamic options

Nika Kastelec

September 8, 2025

## 1 Introduction

The goal of our stay in Prague was to document and test the new options for the dynamic configuration that have been implemented over the past few years, mostly by Fabrice Voitus. Since these options appeared in different code cycles, it was necessary to compare the implementation of each new feature. In the following section, we briefly describe the options, while more detailed documentation can be found in the accompanying file "Proposal for the setting of new dynamic options for high resolution runs in DEODE". This will be followed by the results of various tests performed within the DEODE scripting system.

## 2 Summary of new options

### 2.1 Elimination of the linear system up to horizontal divergence

In the ICI time scheme, the system is first reduced to a single variable. In the hydrostatic model, this variable is the horizontal divergence. In the non-hydrostatic model, it has so far been the vertical divergence, but with the new option LSI_NHEE = T, it is also the horizontal divergence. This has no meteorological impact, but it does not give bit-identical results.

### 2.2 New vertical divergence variable

The formulation of the vertical divergence variable was revised. In the previous definition ($d_4$) (NVDVAR = 4), the nonlinear terms vanish in the linear model, while the new definition ($d_5$) (NVDVAR = 5) retains them consistently. With this change, the evolution equations remain the same in both the full and linear models, with the only difference appearing in the transformation from vertical velocity to divergence.

### 2.3 Consistent moisture inclusion in the definition of "d" and of the X-term

With L_RDRY_VD and L_RDRY_NHX in NAMDYNA, one can specify whether the vertical divergence and the $X^S$ term are defined using the dry gas constant. When enabled, both quantities are treated consistently throughout the code. In all cases, the true 3D divergence must still be correctly calculated by subtracting the appropriate $X^S$ and retaining the moist definition of divergence.

### 2.4 Better bottom boundary condition for the vertical velocity variable

A modified vertical velocity $W$ is introduced, defined as $gW = gw+Y$, where $Y$ depends on a prescribed monotonic vertical function $S(\eta)$.This function is chosen so that $S(\eta)\nabla\Phi_S$ matches $\nabla\Phi$ in a stationary

isothermal hydrostatic atmosphere, where $\eta$ denotes the vertical coordinate, $\Phi$ the geopotential. With this formulation, $W$ behaves like $w$ at the top and like $\dot{\eta}$ at the bottom, with rigid boundary conditions $W_S = 0$ and $\dot{W}_S = 0$. The associated horizontal gradients are adjusted accordingly and the vertical divergence variables are modified by an additional term $X_w$, which represents the contribution of the new velocity definition.

### 2.5 Treatment of the orographic part of the vertical divergence variable X-term

The variable $d$ is defined as the sum of the true vertical divergence and an additional $X$-term, which combines contributions from $X^S$, $X^d$, and $X^w$ depending on various logical options. Under ND4SYS = 0, the $X$-term is calculated directly at the beginning of the time step in the grid point space, avoiding the transformation to the spectral space and reducing CPU usage, while other ND4SYS options may transform $X$ for implicit calculations or handle it explicitly. Horizontal derivatives of the $X$-term are generally not needed, except in some turbulence-related options, and the overall motivation of these modifications is to maintain consistency while potentially reducing computational cost.

### 2.6 Blended hydrostatic-fully-elastic system

The equation system is rewritten using a control parameter $\delta$, which scales the contributions of non-hydrostatic and fully elastic terms. Starting with $\delta = 0$, one can begin with the hydrostatic model and gradually transition to the fully elastic system as $\delta$ approaches 1. Intermediate values of $\delta$ allow for a blended system that filters fast-moving waves of little meteorological relevance, enhancing the numerical stability of the time-stepping scheme.

## 3 AROME validation experiment with new dynamics

As part of the DEODE monthly validation runs, we performed validation of the AROME model with the new dynamics. The experiment was carried out on a domain of $1500 \times 1500$ grid points, with a horizontal resolution of 500 m and 90 vertical levels, using single precision. The simulations were computed on the ECMWF ATOS system in Bologna. We used the tag version available at https://github.com/destination-earth-digital-twins/IAL/releases/tag/CY49t2-v1.8.0, including adaptations from the PR at https://github.com/destination-earth-digital-twins/IAL/pull/148. The default DEODE settings for AROME were applied.

Forecasts were run daily from 1 November 2024 to 30 November 2024, starting at 00 UTC with a 48-hour forecast range. This setup allows for a direct comparison of the new dynamics against the reference configuration. The changes for dynamic applied in the namelist are summarized in Table 1, which shows the differences between the original and the modified settings. Figures 1 present the RMSE and BIAS scores for the monthly forecasts of T2m, S10m, and PMSL. We focus on comparing the default CY49t2_AROMEsp run (purple) with the CY49t2_AROMEspnd run (red) using the new dynamics. The differences are very small, as expected. The legend can be found in Table 2.

Unfortunately, available measurements in the upper atmosphere are quite limited, making the plots rather uninformative. Comparison of the norms is presented in Section 6, as it turns out that unexpected deviations appear in the non-hydrostatic variables.

## 4 Blended hydrostatic-fully-elastic approach

We also tested the NHHY approach, where the model is initialized in a hydrostatic configuration and, over the course of three model runs, gradually transitions to the non-hydrostatic regime. Conceptually, this method relies on rewriting the governing equation system using a control parameter $\delta$, which scales the contributions of the non-hydrostatic and fully elastic terms. For this experiment, we used cy48t3_deode with the settings NSTART_NHHY = 120 and NSTOP_NHHY = 480. Given the model time step of 15 s, the simulation started as hydrostatic for the first 30 minutes. Over the following 2.5 hours, the model gradually transformed into a fully non-hydrostatic configuration. There are some plots of norms for divergence (Figure 2) and pressure departure (Figure 3). We observe that,

```
&NAMDYNA
    LCOMADH = .TRUE.,
    LCOMADV = .FALSE.,
    LCOMAD_GFL = .TRUE.,
    LCOMAD_SP = .TRUE.,
    LCOMAD_SPD = .TRUE.,
    LCOMAD_SVD = .TRUE.,
    LCOMAD_T = .TRUE.,
    LCOMAD_W = .TRUE.,
    LGWADV = .TRUE.,
    LNESC = .TRUE.,
    LNHEE = .TRUE.,
    LPC_CHEAP = .TRUE.,
    LPC_FULL = .TRUE.,
    LRDBBC = .FALSE.,
    LSETTLS = .FALSE.,
    LSETTLST = .TRUE.,
    LSLAG = .TRUE.,
    LSLHD_GFL = .FALSE.,
    LSLHD_OLD = .FALSE.,
    LSLHD_SPD = .FALSE.,
    LSLHD_SVD = .FALSE.,
    LSLHD_T = .FALSE.,
    LSLHD_W = .FALSE.,
    LSPRT = .TRUE.,
    LTWOTL = .TRUE.,
    ND4SYS = 2,
    NPDVAR = 2,
    NVDVAR = 4,
    SLHDEPSH = 0.08,
    SLHDKMAX = 6,
    LSI_NHEE = .FALSE.,
    LBIGW = .FALSE.,
    LSPNHX = .TRUE.,
    L_RDRY_NHX = .FALSE.,
/
```

```
&NAMDYNA
    LCOMADH = .TRUE.,
    LCOMADV = .FALSE.,
    LCOMAD_GFL = .TRUE.,
    LCOMAD_SP = .TRUE.,
    LCOMAD_SPD = .TRUE.,
    LCOMAD_SVD = .TRUE.,
    LCOMAD_T = .TRUE.,
    LCOMAD_W = .TRUE.,
    LGWADV = .TRUE.,
    LNESC = .TRUE.,
    LNHEE = .TRUE.,
    LPC_CHEAP = .TRUE.,
    LPC_FULL = .TRUE.,
    LRDBBC = .FALSE.,
    LSETTLS = .FALSE.,
    LSETTLST = .TRUE.,
    LSLAG = .TRUE.,
    LSLHD_GFL = .FALSE.,
    LSLHD_OLD = .FALSE.,
    LSLHD_SPD = .FALSE.,
    LSLHD_SVD = .FALSE.,
    LSLHD_T = .FALSE.,
    LSLHD_W = .FALSE.,
    LSPRT = .TRUE.,
    LTWOTL = .TRUE.,
    ND4SYS = 0,
    NPDVAR = 2,
    NVDVAR = 5,
    SLHDEPSH = 0.08,
    SLHDKMAX = 6,
    LSI_NHEE = .TRUE.,
    LBIGW = .TRUE.,
    LSPNHX = .FALSE.,
    L_RDRY_NHX = .TRUE.,
/
```

Table 1: Comparison of old (left) and new (right) settings for dynamics in namelist. Red values indicate the changes in the new configuration.

| **Color** | **Model** |
|---|---|
| Pink | CY46h1_HARMONIE_AROME |
| Light green | CY48t3_AROME |
| Blue | CY49t2_ALARO_DP |
| Purple | CY49t2_AROME_SP |
| Red | CY49t2_AROME_SPnd (newdyn) |
| Light gray | CY49t2_HARMONIE_AROME_SP |
| Green | GDT_iekm 4,5km global model |
| Orange | IFS (HRES) 9km global model |

Table 2: Legend of models and colors. Add explanations in the third column.

regardless of whether the blending approach is applied, the spectral norms after NSTOP_NHHY remain very similar for both ALARO and AROME.

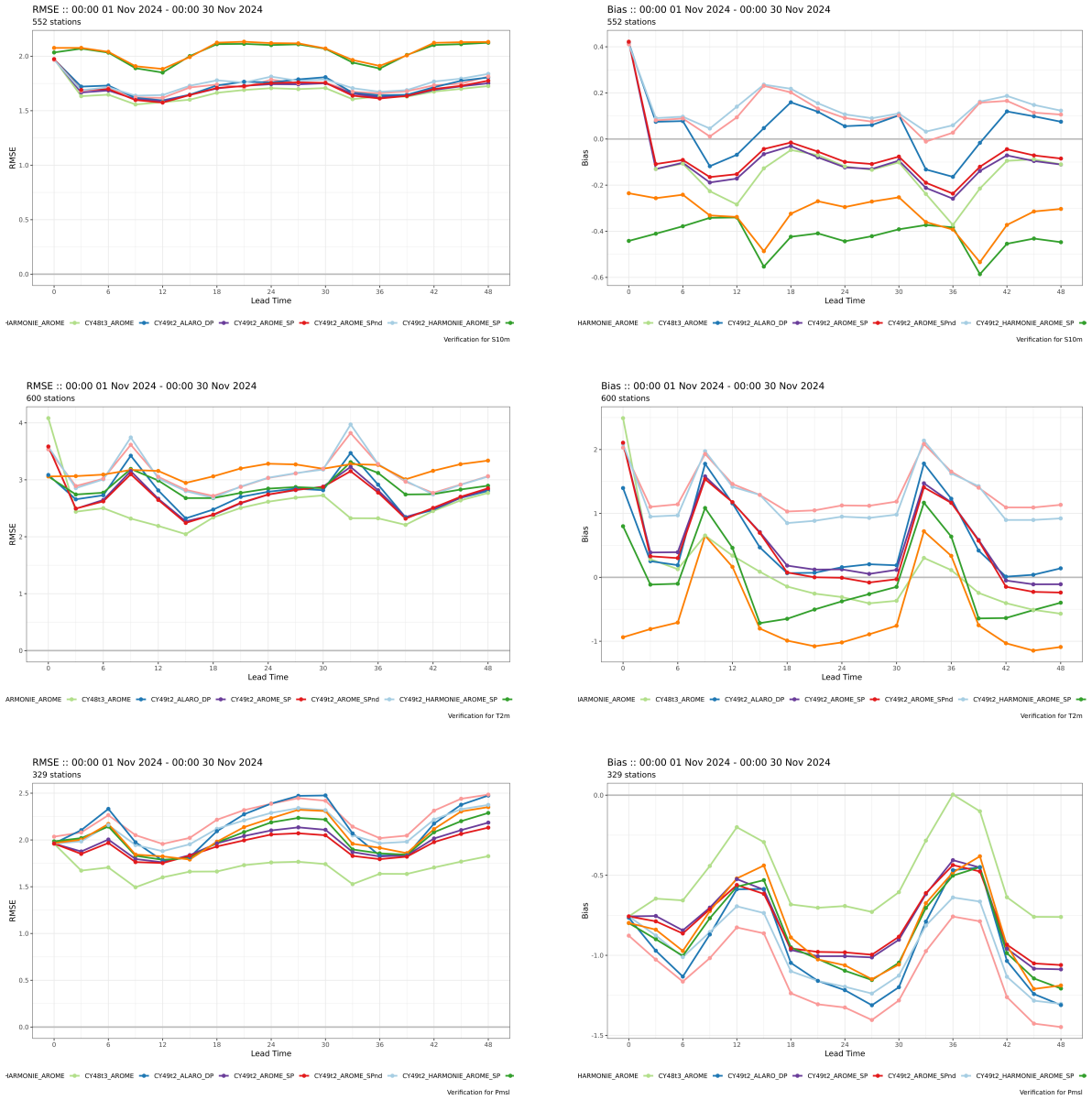


Figure 1: Overview of RMSE and BIAS scores for S10m (first row), T2m (second row), and PMSL(last row). Purple: default run, Red: new dynamics.

# 5 Settings for nudging in AROME

During the testing of the new dynamics, we observed an unexpected behavior of the pressure departure field in the AROME model. At every full hour, the field appeared to be artificially forced toward larger values (see Fig. 4). The effect was most pronounced near the model top when plotting the norms level by level, which led us to suspect the nudging as a possible cause. Further experiments confirmed this, as the peaks disappeared once the spectral nudging at the model top was disabled. To address this issue, we obtained updated nudging settings from our colleagues in France, consistent with those applied in their operational 500-meter model. With these settings, the shape of the mean norm curve of the pressure departure is significantly improved (see Fig. 5). The experiments were performed with cycle cy48t_deode on the Finnish domain, using a 1500×1500 grid at 500 m resolution. A 48-hour integration was conducted starting at 00 UTC on 15 November 2024, coinciding with a period of strong winds. The namelist change is described in Table 3.

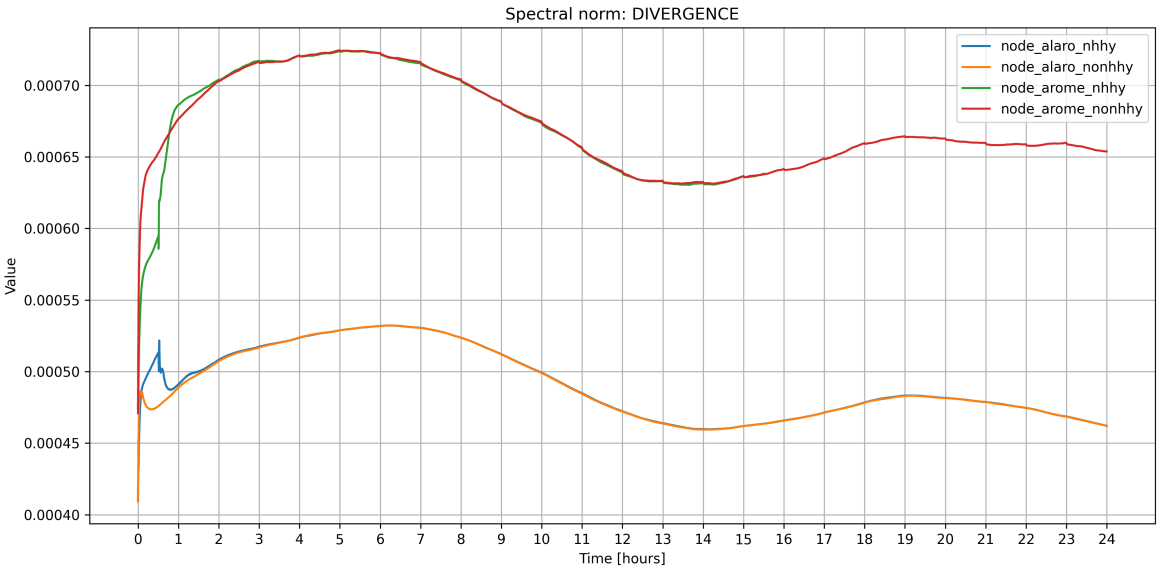


Figure 2: Spectral norms of divergence for ALARO and AROME with and without the NHHY approach. Blue: ALARO with NHHY=T; orange: ALARO with NHHY=F; green: AROME with NHHY=T; red: AROME with NHHY=F.

| | |
|---|---|
| `&NEMELBC0B` | `&NEMELBC0B` |
| `NEFRSPCPL = 1,` | `NEFRSPCPL=1,` |
| `NEK0 = 220,` | `NEK0=20,` |
| `NEK1 = 255,` | `NEK1=30,` |
| `NEN1 = 4,` | `NEN1=4,` |
| `NEN2 = 8,` | `NEN2=8,` |
| `SPNUDDIV = 0.3,` | `SPNUDDIV=0.01,` |
| `SPNUDQ = 0.0,` | `SPNUDQ=0.,` |
| `SPNUDT = 0.3,` | `SPNUDT=0.01,` |
| `SPNUDVOR = 0.3,` | `SPNUDVOR=0.01,` |
| `TEFRCL=3600.,` | `TEFRCL=3600.,` |

Table 3: Comparison of old (left) and new (right) settings in namelist.

# 6 Some problems in DEODE code

Looking at the figures below (Figure 6 - 11), showing the average spectral norms, we observe that for ALARO these hardly change when the dynamic settings are modified. In contrast, for AROME, unexpected differences appear in the norms of the non-hydrostatic variables (mostly in pressure departure), which are not anticipated from the code changes. Since ALARO and AROME also differ in model physics, we decided to carry out further tests using adiabatic models.

The adiabatic experiments produced similar results. Since the value of VESL in AROME is set to 0.05, while in ALARO it is 0, we tested whether adjusting VESL in AROME to 0 would affect the outcome. Indeed, with VESL is 0, the differences between the old and new dynamics disappeared. Conversely, we confirmed that setting VESL $> 0$ in ALARO introduces discrepancies between the dynamic configurations (see Fig. 13 and 14). A similar behavior was also observed in cycle cy48t3. The reason for this remains unclear, and further inspection of the code integrated into the DEODE repository will be required, as such differences do not appear with the upstream (non-DEODE) code.

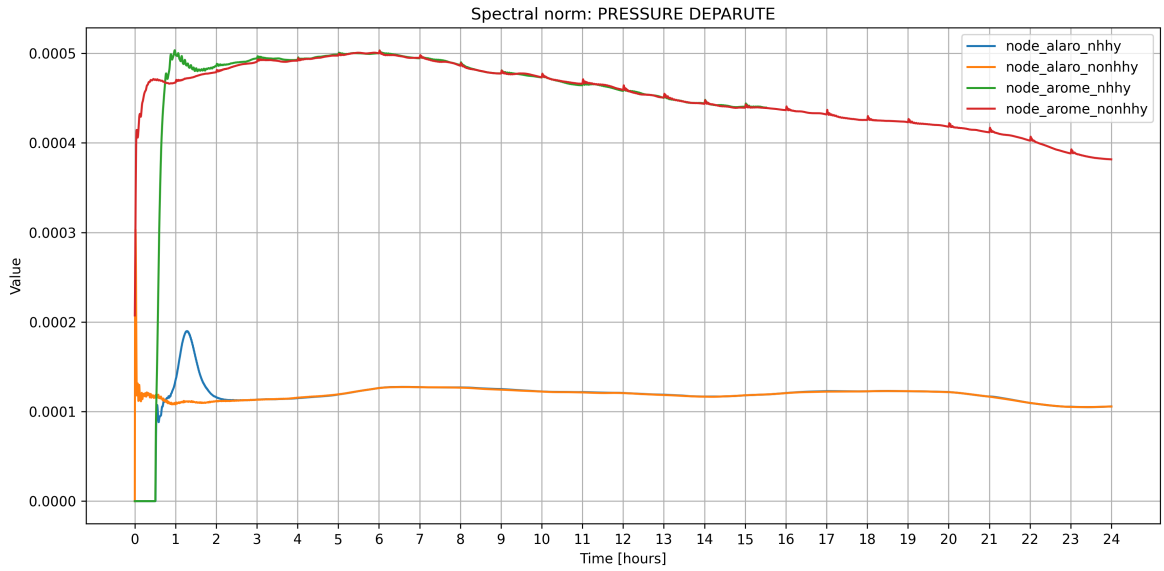


Figure 3: Spectral norms of pressure departure for ALARO and AROME with and without the NHHY approach. Blue: ALARO with NHHY=T; orange: ALARO with NHHY=F; green: AROME with NHHY=T; red: AROME with NHHY=F.

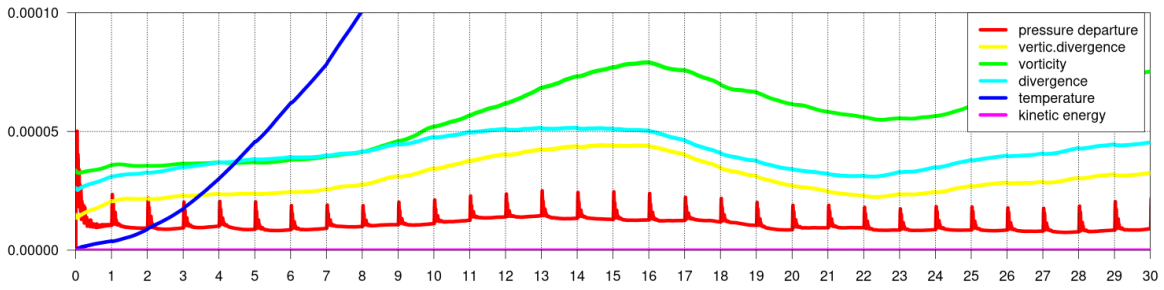


Figure 4: Average norms with old set of nudging configuration.

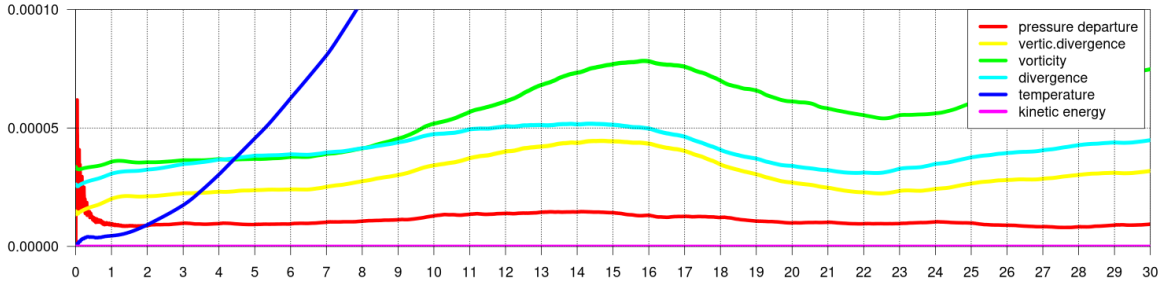


Figure 5: Average norms with new set of nudging configuration.

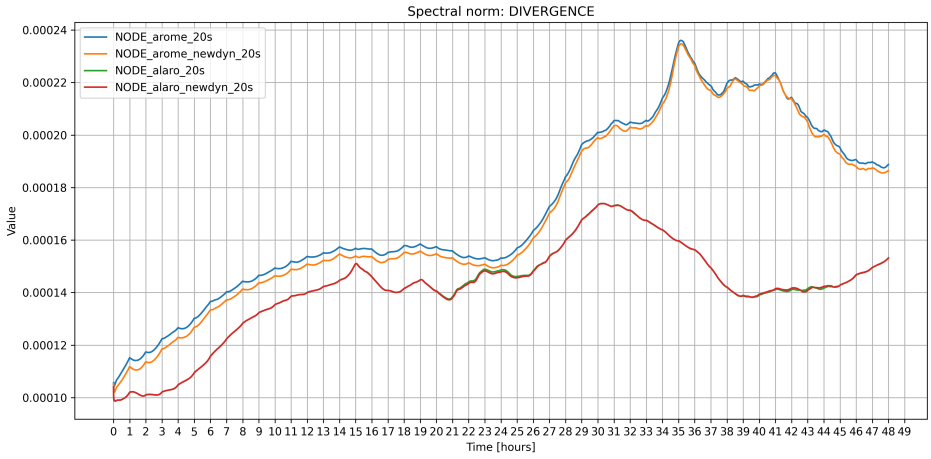


Figure 6: Spectral norms of divergence comparing ALARO and AROME with old and new dynamics.

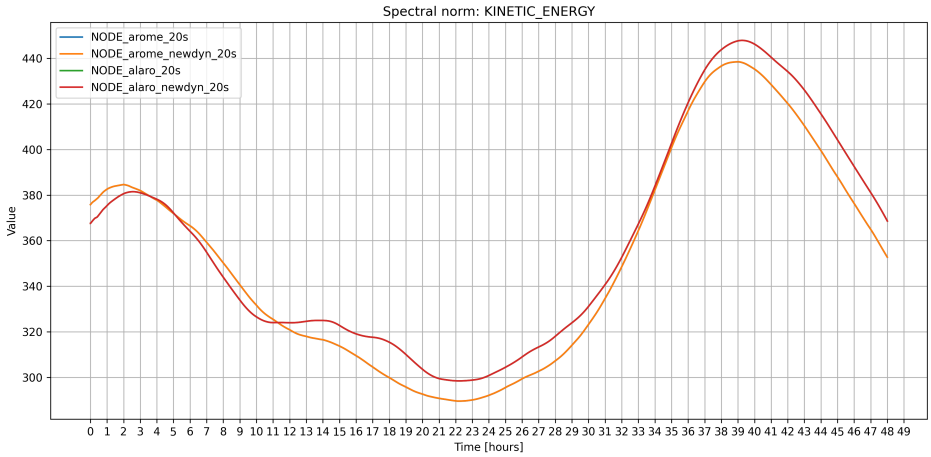


Figure 7: Spectral norms of kinetic energy comparing ALARO and AROME with old and new dynamics.

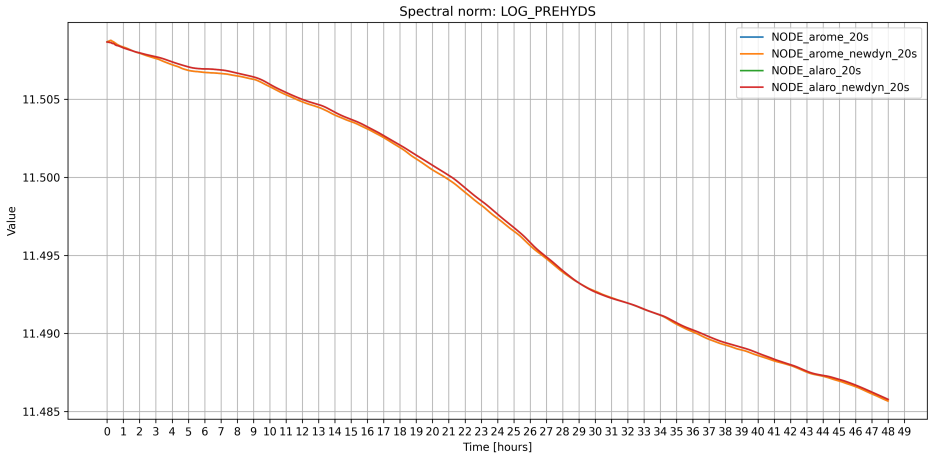


Figure 8: Spectral norms of log hydrostatic pressure comparing ALARO and AROME with old and new dynamics.

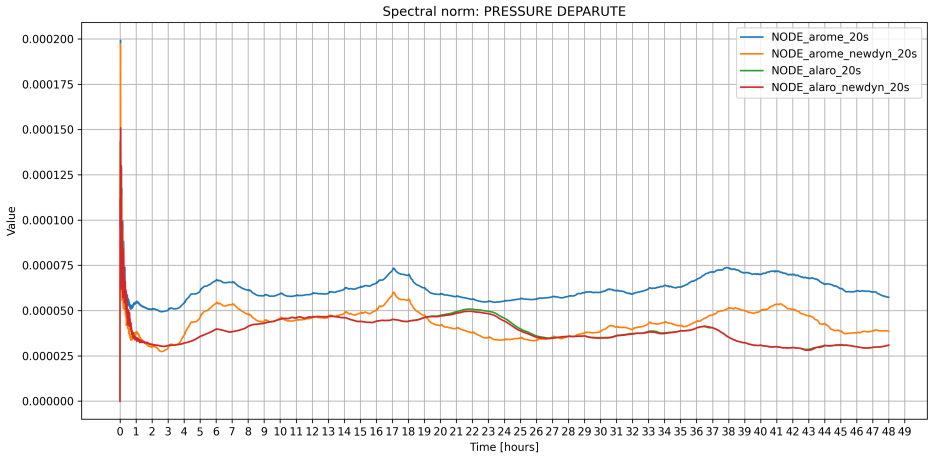


Figure 9: Spectral norms of pressure departure comparing ALARO and AROME with old and new dynamics.

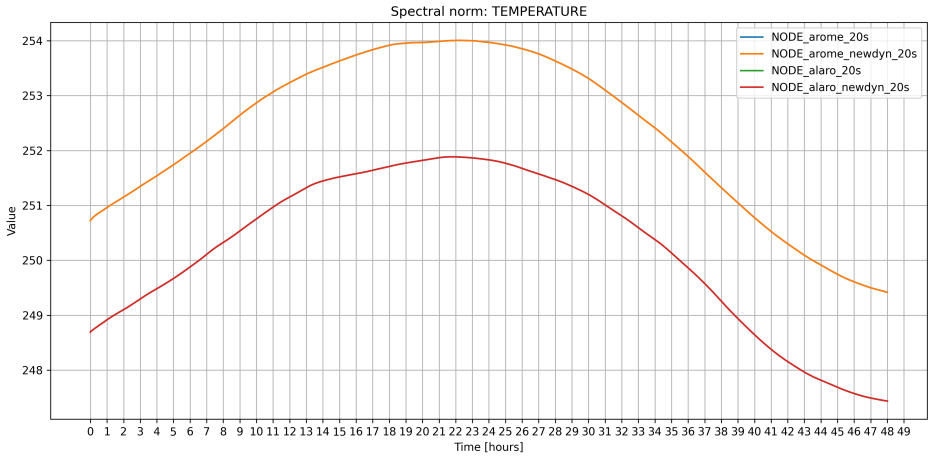


Figure 10: Spectral norms of temperature comparing ALARO and AROME with old and new dynamics.

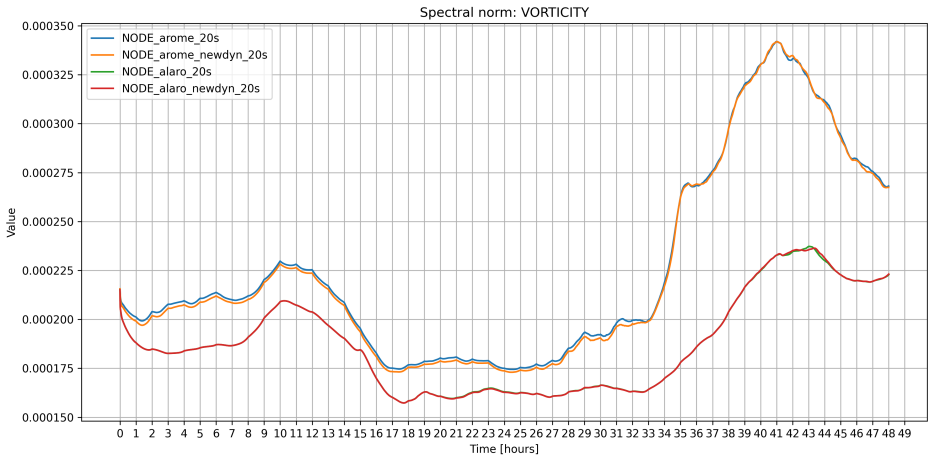


Figure 11: Spectral norms of vorticity comparing ALARO and AROME with old and new dynamics.

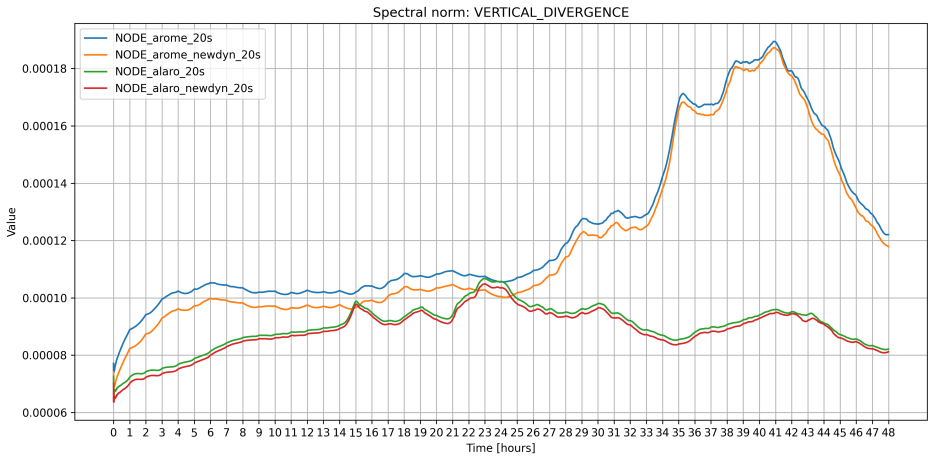


Figure 12: Spectral norms of vertical divergence comparing ALARO and AROME with old and new dynamics.

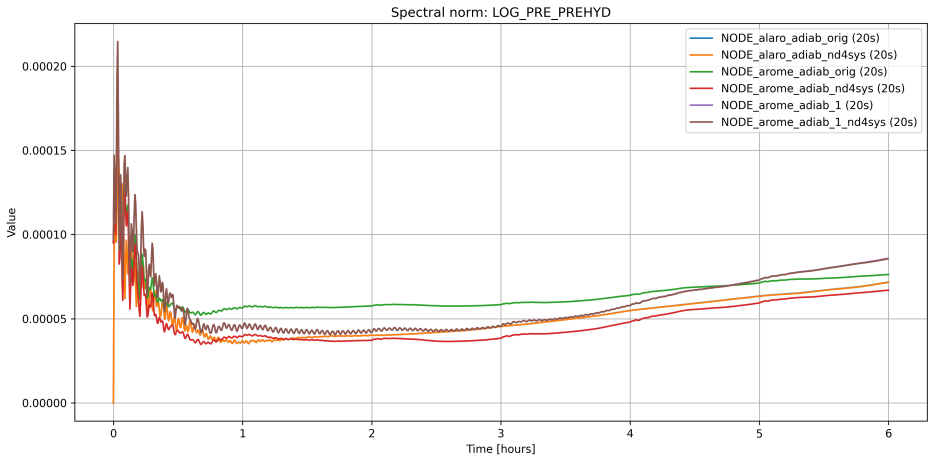


(a) The blue and orange lines coincide.

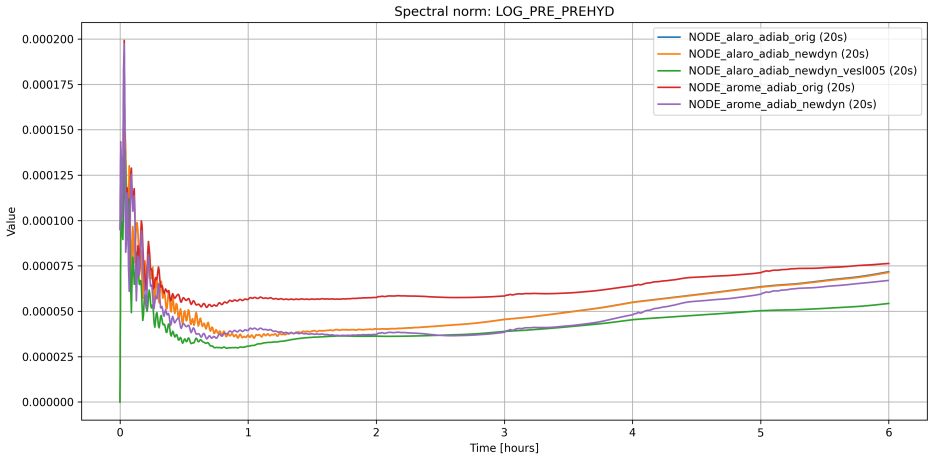


(b) The blue and green lines coincide.

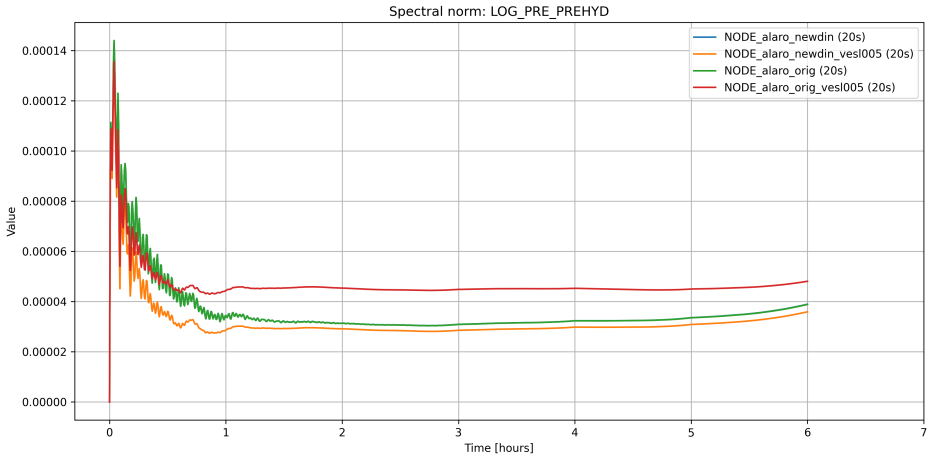


(c) The blue and green lines coincide.

Figure 13: Norms for the pressure departure. Comparing VESL=0 and 0.005 and the new and old dynamics. Top: AROME cy49t2_deode adiabatic, middle: ALARO cy49t2_deode adiabatic, bottom: ALARO cy48t3_deode full model.

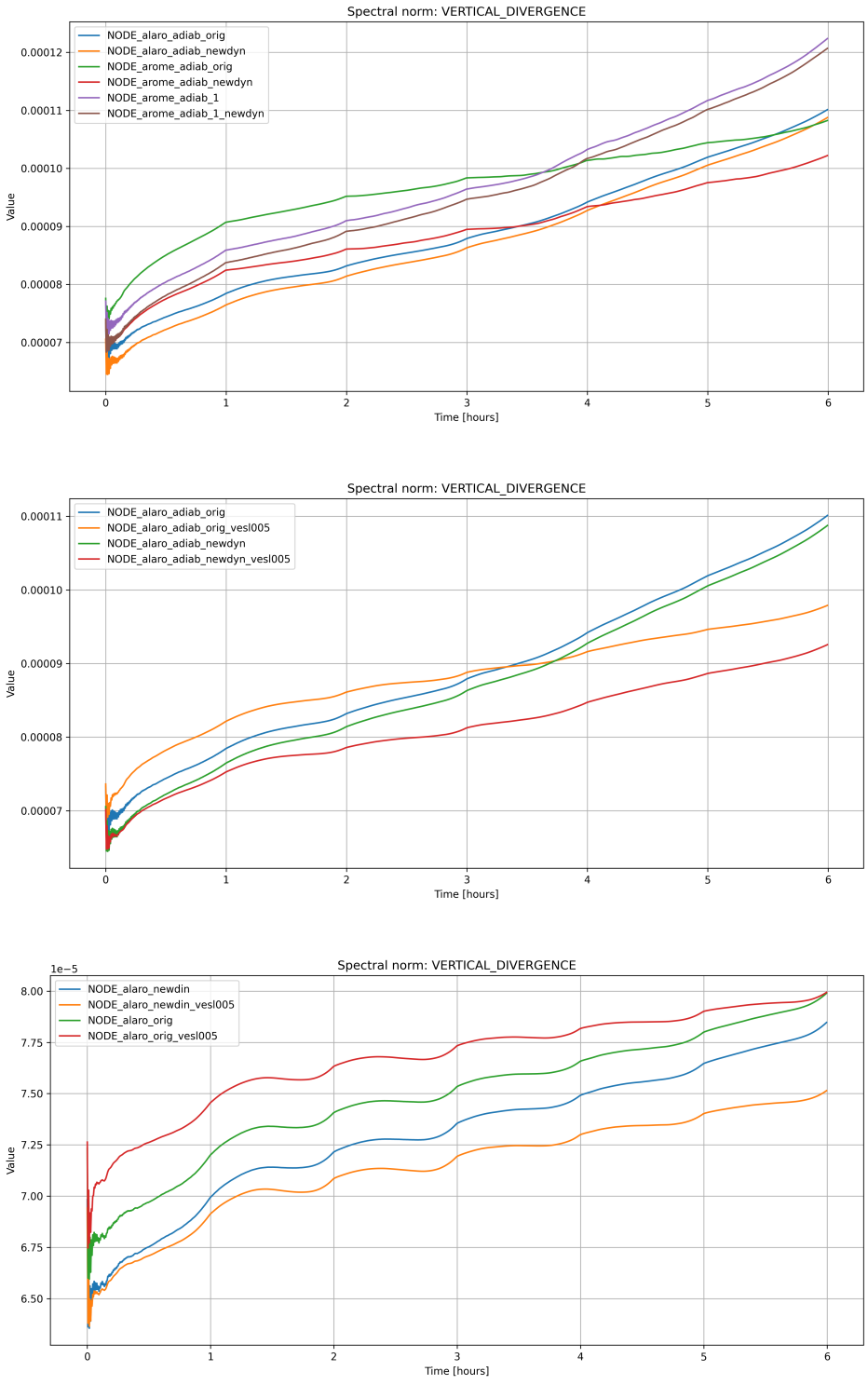


Figure 14: Norms for the vertical divergence. Comparing VESL=0 and 0.005 and the new and old dynamics. Top: AROME cy49t2_deode adiabatic, middle: ALARO cy49t2_deode adiabatic, bottom: ALARO cy48t3_deode full model